

CONCEPTUAL DESIGN OF THE CAVITY MECHANICAL SYSTEM FOR CAVITY-BASED X-RAY FREE ELECTRON LASER*

D. Shu[†], S. Kearney, J. Anton, S. Mashrafi, Yu. Shvyd'ko, R. Lindberg, W. Jansma, W. Toter, X. Shi, L. Assoufid, M. White, K-J. Kim, Argonne National Laboratory, Lemont, IL 60439, USA
 T. Tan, D. Zhu, G. Gassner, F-J. Decker, H-D. Nuhn, H. Bassan, G. Marcus, Z. Huang, SLAC National Accelerator Laboratory, Menlo Park, CA 94025, USA

Abstract

The concept behind the cavity-based X-ray FELs (CBXFELs) such as the X-ray free-electron laser oscillator (XFEL) and the X-ray regenerative amplifier free-electron laser (XRAFEL) is to form an X-ray cavity with a set of narrow bandwidth diamond Bragg crystals. Storing and recirculating the output of an amplifier in an X-ray cavity so that the X-ray pulse can interact with following fresh electron bunches over many passes enables the development of full temporal coherence [1, 2]. One of the key challenges to forming the X-ray cavity is the precision of the cavity mechanical system design and construction. In this paper, we present conceptual design of the cavity mechanical system that is currently under development for use in a proof-of-principle cavity-based X-ray free electron laser experiment at the LCLS-II at SLAC.

INTRODUCTION

X-ray free electron lasers (XFELs) based on Self-Amplified Spontaneous Emission (SASE) [3] are demonstrated extremely bright, transversely coherent, ultrashort X-ray pulses for the investigation of ultrafast chemical and physical processes at the LCLS and other XFEL user facilities around world [4-6]. However, the single-pass SASE FEL amplifiers have poor longitudinal coherence.

Since 2019, collaboration between Argonne National Laboratory (ANL) and SLAC National Accelerator Laboratory has been established to design and construct a cavity mechanical system for use in a proof-of-principle cavity-based X-ray free electron laser experiment at the LCLS-II at SLAC. The experiment aim is to obtain temporally-coherent XFEL pulses by storing and recirculating the output of an amplifier in an X-ray cavity so that the X-ray pulse can interact with the following fresh electron bunches over many passes [1, 2].

A set of four diamond crystals with narrow Bragg bandwidth will provide high reflectivity and mono-chromatization to form a rectangular X-ray cavity around the first seven LCLS-II undulator units. The rectangular shape is chosen because of the constraints of the available space in the undulator hall. Two aspects of the cavity-based X-ray FELs (CBXFELs) are planned for this experiment: the X-ray free-electron laser oscillator (XFEL) [7] relies on a

low-loss cavity supporting a low-gain free-electron laser, and the X-ray regenerative amplifier free-electron laser (XRAFEL) [8, 9] leverages a high-gain FEL interaction. During the initial experiment, the LCLS-II Cu-linac will produce a pair of electron bunches separated by the cavity-round-trip distance during each linac cycle with a mean energy of 10.3 GeV. Figure 1 shows a schematic diagram of the CBXFEL experiment setup at the LCLS-II at SLAC.

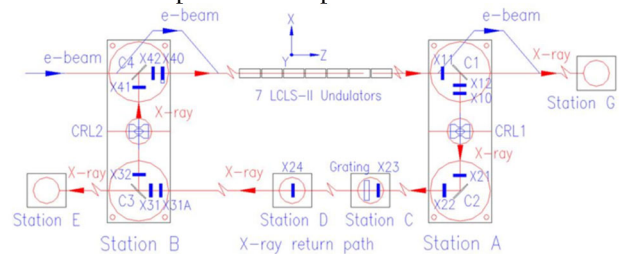


Figure 1: Schematic diagram of the CBXFEL experiment setup at the LCLS-II at SLAC.

EXPERIMENT STATIONS

The mechanical system for the rectangular x-ray cavity of the CBXFEL at LCLS-II includes four sets of diamond crystal holders (C1, C2, C3, and C4) with nanopositioning stages in UHV chambers, see Fig. 2. These nanopositioning stages and vacuum chambers are grouped into two crystal stations (stations A and B), and five diagnostic stations (stations C, D, E, F, and G). Each of the crystal stations shall be integrated with their associated chicane magnets and vacuum systems on the same girder to meet the requirement for LCLS-II e-beam-based alignment operation.

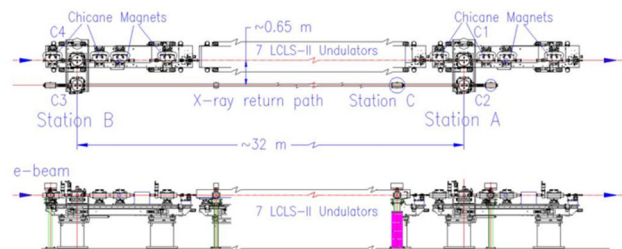


Figure 2: General layout of the cavity mechanical system for the CBXFEL at LCLS-II at SLAC.

The CBXFEL mechanical system also includes a vacuum pipe system as the cavity's X-ray return path. The X-ray diagnostic stations C, D, and E are located in the X-ray return path and its extension line. The X-ray diagnostic station G is located in the LCLS-II experimental station. Since it may not be in the same cavity vacuum system, the X-ray

* This research used resources of the Advanced Photon Source, a U.S. Department of Energy (DOE) Office of Science User Facility at Argonne National Laboratory and is based on research supported by the U.S. DOE Office of Science-Basic Energy Sciences, under Contract No. DE-AC02-06CH11357 (ANL) and DE-AC02-76SF00515 (SLAC).

[†]shud@anl.gov

diagnostic station E and G will be designed separately. Figure 2 shows the general layout of the cavity mechanical system for the ~ 32 m x ~0.65 m rectangular x-ray cavity of the CBXFEL experiment at LCLS-II.

UHV NANOPositionING DESIGN

One of the key challenges to forming the X-ray cavity is the precision of the cavity mechanical system design and construction. Nanopositioning techniques present a significant opportunity to support this state-of-the-art design with ultra-high-vacuum (UHV) compatibility.

Vacuum System Requirement

The LCLS-II undulator segment vacuum chamber needs to be operated at a pressure better than 10^{-6} torr in order to minimize bremsstrahlung and emittance growth. However, the design of vacuum system shall have highest priority on the operation reliability and maintainability to minimize any possible interference to the operations of the LCLS-II XFEL user facility. Similar to the design of the LCLS-I and LCLS-II self-seeding monochromators, the vacuum system of the CBXFEL optomechanical system need to meet typical UHV level cleanliness. Ion pumps are integrated with the CBXFEL vacuum chambers. All-metal manual isolation valves and welded bellows are the vacuum interfaces for the CBXFEL to the LCLS-II vacuum system.

Support and Metrology Reference Systems for Crystal Stations

Support System Based on the LCLS-II beam-based-alignment requirement, each of the diamond crystal station and its associated chicane dipole magnets are supported by a steel girder. As shown in Fig. 3, a special stiffener structure is designed to provide a stable interface between the girder and crystal station Invar base.

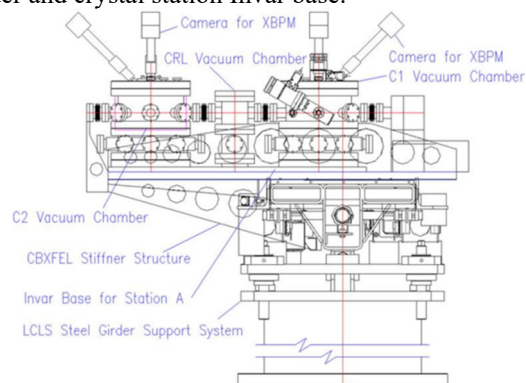


Figure 3: Rear view of the girder and stiffener structure for the CBXFEL diamond crystal station A.

Metrology Reference Base Each of the crystal stations has an Invar base with global survey/alignment fiducial holes outside the vacuum. Metrology reference frames are established inside the vacuum enclosure to mount the laser interferometer's fiber-optics frontends and the capacitive sensor's sensing heads.

To mount both C1 and C2 in-vacuum Invar metrology frames directly to a common Invar base in air with limited

space available for CBXFEL, a special flexure UHV interface has been developed for an Invar base near-zero-length feedthrough as shown in Fig. 4 [10]. The flexure interface structure is strong enough to hold the vacuum force and flexible enough to survive the thermal expansion stresses incurred during an 80 – 100 degree Celsius bakeout process for UHV preparation.

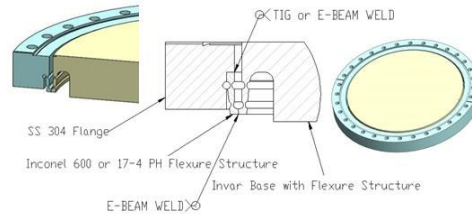


Figure 4: Invar base near-zero-length feedthrough for CBXFEL diamond crystal UHV Invar metrology frames.

Long Range Laser Interferometer

A customized commercial multichannel laser interferometer system is integrated as a part of the opto-mechanical system to monitor the cavity total length and XBPM locations during the system installation, commissioning and operation processes. With the laser interferometer's real-time measurements, the nanopositioning stages are able to compensate the thermal drifting of the mechanical system with a closed-loop feedback control.

The customized Hexagon™ Etalon™ absolute multiline laser interferometer system has a maximum measuring range larger than 32 meters with measurement uncertainty better than 0.4 micron/m [11, 12].

Capacitive Sensor

Commercial miniaturized capacitive sensors are applied in the CBXFEL mechanical system to provide repeatable absolute measurement in a short distance to ensure the traceability of the metrology structure during the CBXFEL mechanical system assembly, installation, commissioning and operation processes. A typical sensor has a measuring range ~ 2.0 mm with measurement resolution 5 - 10 nm.

Stages for Diamond Crystal Manipulation

As shown in Fig. 5, the nanopositioning stages group for diamond crystal manipulation includes four precision flexure stages and three commercial miniaturized PZT-motor-driven precision bearing stages [13].

The flexure linear and tip-tilting stages were designed based on the weak-link mechanism technique developed by Advanced Photon Source (APS) for synchrotron radiation applications [14-19]. The newly designed UHV-compatible tip-tilting weak-link stages for CBXFEL aim to have extended travel range up to 1.5 degree with 10 – 30 nrad resolution. With an end-target positioning closed-loop dynamic correction, the new linear flexure stages are designed to have maximum angular crosstalk below 100 nrad over ±300 μm travel range. Design specifications are listed in Table 1.

A diamond crystal holder is mounted on the top of the stage group. The holder is similar to the APS designed

diamond crystal holder for European-XFEL self-seeding monochromator. A heater with thermostat is installed on the holder to keep an even temperature for all the diamond crystals in the cavity system.

To minimize the heat consumption of the stages in a vacuum environment, all of the nanopositioning stages are driven by PZT-based motors or actuators.

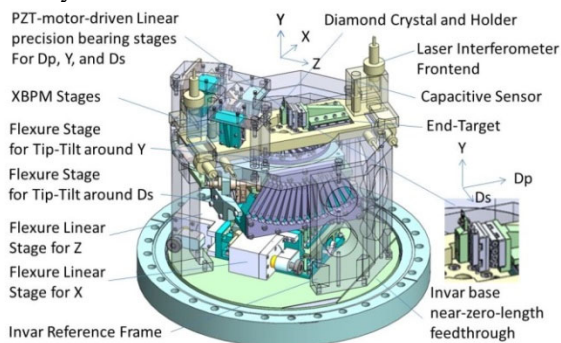


Figure 5: Nanopositioning stages group for diamond crystal manipulation with in-vacuum Invar reference frame

Table 1: Design Specifications for Crystal Stages

Stage name	Travel Range	Resolution
Linear flexure stage for X and Z (coarse)	1000 micron	50 nm
Linear flexure stage for X and Z (fine, optional)	15 micron	5 nm
Tip-Tilt flexure stage for around Y and Ds (coarse)	26 mrad	350 nrad
Tip-Tilt flexure stage for around Y and Ds (fine)	0.1 mrad	20 nrad
Linear miniaturized stage for Dp, Y, and Ds	12 mm	50 nm

Stages for XBPMs and CRLs

The nanopositioning stages group for X-ray beam position monitors (XBPMs) and compound refractive lenses (CRLs) includes two miniaturized PZT-motor-driven precision bearing stages.

Survey and Alignment of Stages

The home position of all stage groups is measured by CMM during the final assembly process with 3 μm uncertainty with respect to the reference base global survey/alignment fiducials. Positions are traceable using capacitive sensors for flexure stages and grating encoders for bearing stages.

Interface to the CBXFEL Control System

An integrated cavity optics dynamic positioning database (ICO-DPD) will be established as one of the interface between the CBXFEL mechanical and control system. The detailed ICO-DPD documentation will ensure uniformity and reduce system errors on the units, coordinates, names, tooling ball standards and etc. for cavity crystal motion control and beam diagnostics use.

The ICO-DPD will integrate the measurement results, including environment condition of the measurement, from digital measuring machine and digital microscope during the component manufacturing and sub-assembly process. With absolute and relative encoders mounted on the invar base and reference frame, the ICO-DPD will also record every movement of the cavity optical components

positions related to system fiducial positions on the invar base during the final assembly, installation, and survey/alignment process. The ICO-DPD could also be linked to the SLAC beam based alignment system.

SUMMARY

A cavity mechanical system that is currently under development for use in a proof-of-principle CBXFEL experiment at the LCLS-II is presented in this paper. As a part of the first article development activities, pilot flexure stages are designed, constructed, and started preliminary testing at the APS. Figure 6 shows a photograph of the pilot flexure stages group for diamond crystal manipulating. Figure 7 shows a preliminary test result for the tip-tilt flexure stage for the angular adjustment around the diamond crystal surface horizontal Axis Ds, which shows a 3-up and 3-down open-loop steps with resolution ~ 20 nrad. Further test is planned to demonstrate the stages' closed-loop dynamic correction capability with end-target laser interferometer and capacitive sensors. A final design review for the CBXFEL cavity mechanical system is scheduled at the end of August 2021.



Figure 6: A photograph of the pilot nanopositioning stages for CBXFEL diamond crystal manipulation.

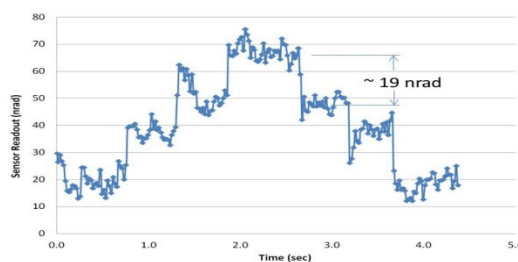


Figure 7: A preliminary open-loop test result for the tip-tilt flexure stage for the angular adjustment around the diamond crystal surface horizontal Axis Ds.

ACKNOWLEDGEMENTS

The authors would like to acknowledge the management support from Argonne National Laboratory and SLAC National Accelerator Laboratory.

REFERENCES

- [1] K-J. Kim *et al.*, "Test of an x-ray cavity with double bunches from the LSLC Cu-Linac," in *Proc. IPAC'19*, Melbourne, Australia, May 2019, pp. 1887-1890.

<https://doi.org/10.18429/JACoW-IPAC2019-TUPRB096>

[2] G. Marcus *et al.*, “Cavity-based free-electron laser research and development: a joint Argonne National Laboratory and SLAC National Laboratory collaboration.” in *Proc. FEL2019*, Hamburg, Germany, August 2019, pp. 282-287. <https://doi.org/10.18429/JACoW-FEL2019-TUD04>

[3] A. Kondratenko and E. Saldin, “Generation of coherent radiation by a relativistic electron beam in an undulator,” *Part. Accelerators*, vol. 10, pp. 207-216, 1980. <http://cds.cern.ch/record/1107977/files/p207.pdf>

[4] <https://www.xfel.eu>

[5] <https://pal.postech.ac.kr>

[6] <http://xfel.riken.jp>

[7] K.-J. Kim, Y. Shvyd'ko, and S. Reiche, “A proposal for an x-ray free-electron laser with an energy-recovery linac,” *Phys. Rev. Lett.*, vol. 100, p. 244802, 2008. doi:<https://doi.org/10.1103/PhysRevLett.100.244802>

[8] Z. Huang and R. D. Ruth, “Fully coherent x-ray pulses from a regenerative-amplifier free-electron laser,” *Phys. Rev. Lett.*, vol. 96, p. 144801, 2006. doi:<https://doi.org/10.1103/PhysRevLett.96.144801>

[9] G. Marcus *et al.*, “Refractive guide switching a regenerative amplifier free-electron laser for high peak and average power hard x rays,” *Phys. Rev. Lett.*, vol. 125, p. 254801, 2020. doi:<https://doi.org/10.1103/PhysRevLett.125.254801>

[10] D. Shu, S. Kearney, J. Anton, W. Toter, “Method and Mechanical Design of a Flexure Interface for Ultra-High-Vacuum Nanopositioning Invar Base Near-Zero-Length Feed-through,” U.S. Patent application #17/346537 for ANL-IN-20-092.

[11] John Dale *et al.*, “Multi-channel absolute distance measurement system with sub ppm-accuracy and 20 m range using frequency scanning interferometry and gas absorption cells,” *Opt. Express*, vol. 22, iss. 20, pp. 24869-24893, 2014. <https://doi.org/10.1364/OE.22.024869>

[12] <https://www.etalonproducts.com/en/products/lasertracer/>

[13] <http://www.smaract.com>

[14] D. Shu, T. S. Toellner, and E. E. Alp, “Modular overconstrained weak-link mechanism for ultraprecision motion control,” *Nucl. Instrum. Methods Phys. Res., Sect. A*, vols. 467-468, pt. 1, pp. 771-774, 2001. [https://doi.org/10.1016/S0168-9002\(01\)00499-5](https://doi.org/10.1016/S0168-9002(01)00499-5)

[15] D. Shu, T. S. Toellner, and E. E. Alp, “Redundantly constrained laminar structure as weak-link mechanisms,” U.S. Patent granted No. 6,607,840, 2003.

[16] D. Shu *et al.*, “Applications of laminar weak-link mechanisms for ultraprecision synchrotron radiation instruments,” *AIP Conf. Proc.*, vol. 879, pp. 1073-1076, 2007. <https://doi.org/10.1063/1.2436249>

[17] D. Shu *et al.*, “Mechanical design of a flexural nanopositioning stage system for hard x-ray nanofocusing at the Advanced Photon Source 32-ID-C station,” in *Proc. SPIE 11112, X-Ray Nanoimaging: Instruments and Methods IV*, San Diego, CA, USA, August 2019, p. 111120N. <https://doi.org/10.1117/12.2529384>

[18] S. Narayanan *et al.*, “Design and performance of an ultra-high-vacuum-compatible artificial channel-cut monochromator,” *J. Synchrotron Radiat.*, vol. 15, pp. 12-18, 2008. doi:10.1107/S090904950705340X

[19] X. Dong, D. Shu, and H. Sinn, “Design of a cryo-cooled artificial channel-cut crystal monochromator for the European XFEL,” *AIP Conf. Proc.*, vol. 1741, p. 040027, 2016. <https://doi.org/10.1063/1.4952899>